

Griffiths singularities and magnetoresistive manganites

M. B. Salamon*

Department of Physics, University of Illinois, 1110 West Green Street, Urbana, Illinois 61801, USA

S. H. Chun†

Department of Physics, Sejong University, Seoul 143-747, Korea

(Received 14 January 2003; revised manuscript received 24 March 2003; published 9 July 2003)

The large, so-called colossal magnetoresistivity of doped LaMnO_3 has attracted considerable attention, but is only one unusual feature of the ferromagnetic transition in these compounds. We examine in this paper the progression of magnetic and thermodynamic behavior as the transition temperature is made to vary from 360 K to 218 K by changing the divalent dopant. Single crystals of $\text{La}_{0.7}\text{Sr}_{0.3}\text{MnO}_3$, as is well known, show modest magnetoresistivity and conventional critical behavior. $\text{La}_{0.66}\text{Pb}_{0.34}\text{MnO}_3$, and to an even greater extent, $\text{La}_{0.7}\text{Ca}_{0.3}\text{MnO}_3$, have unusual magnetic properties extending more than 100 K above the transition. We treat the properties of the latter samples in the context of a Griffiths phase in which the transition temperature is depressed from its maximum value T_C by random bond-angle bending.

DOI: 10.1103/PhysRevB.68.014411

PACS number(s): 75.47.Gk, 75.40.-s, 75.47.Lx

I. INTRODUCTION

The properties of AMnO_3 , where A is a mixture of trivalent lanthanides and divalent ions, have intrigued researchers for decades.¹ The parent compound, LaMnO_3 , crystallizes in a slightly distorted perovskite structure and is an antiferromagnetic insulator with a Néel temperature $T_N \approx 130$ K. When the concentration of divalent atoms (Ca, Sr, Ba, Pb) substituted for La (A -site substitution) exceeds $\approx 1/8$, the low-temperature phase is ferromagnetic and metallic. The Curie temperature depends strongly on the concentration and ionic size of the substituent² and, perhaps most significantly, on the ionic-size variance of A -site atoms.³ The highest Curie temperature, $T_C \approx 360$ K, is achieved with Sr doping at a concentration close to $3/8$, that is, for $\text{La}_{5/8}\text{Sr}_{3/8}\text{MnO}_3$. At this concentration, the material is metallic in both paramagnetic ($T \geq 360$ K) and ferromagnetic phases, and the effect of magnetic fields on the electrical resistivity is not dramatic. The ferromagnetic/paramagnetic transition is entirely normal, by which we mean that the magnetization can be described by critical exponents very close to those expected for a three-dimensional (3D) Heisenberg ferromagnet.⁴

The conventional picture for this system is based on the *double-exchange* mechanism proposed by Zener.⁵ Each divalent substituent converts a Mn^{3+} ion to Mn^{4+} , with the outermost (e_g) electron on the Mn^{3+} site resonating with a neighboring Mn^{4+} via the intervening oxygen atom. Because of strong Hund's-rule coupling, the double-exchange transfer is favored when neighboring core spins are aligned, leading to ferromagnetism. When the substitution level is sufficiently high, the holes doped into this system form a fully spin-polarized (half-metallic) band. As the $S = 3/2$ core (t_{2g}) spins disorder with increasing temperature, the resistivity increases and, near the Curie temperature, exhibits substantial—though not dramatic—magnetoresistance. This picture describes $\text{La}_{5/8}\text{Sr}_{3/8}\text{MnO}_3$ reasonably well.⁶

Changing the Sr content away from $\text{La}_{5/8}\text{Sr}_{3/8}\text{MnO}_3$, substituting Ca or other divalent atoms for Sr at the same concentration, and even substituting other lanthanides for La

sharply decreases T_C and dramatically changes the nature of the paramagnetic/ferromagnetic transition. The resistivity in the paramagnetic phase increases exponentially with decreasing temperature, peaks somewhat above T_C , and then decreases sharply in the ferromagnetic phase. The resistivity peak shifts to higher temperature with increasing field, giving rise to the dramatic field-dependent resistivity that has been termed colossal magnetoresistance (CMR). A calculation of the resistivity within the context of the double-exchange model⁷ provided strong evidence that a localizing mechanism beyond that model was necessary to explain these large field- and temperature-dependent changes, and there is now strong theoretical⁸ and experimental⁹ evidence that polaron formation and accompanying self-trapping of electrons play essential roles. As the average ionic size of A -site atoms decreases toward that of La ($r_A = .1216$ nm), the transition temperature decreases and the exponential increase in resistivity with temperature makes the drop to metallic resistivity at T_C ever more dramatic. A powerful argument can be made that the smaller the A -site atom the greater the distortion of the crystal from the cubic perovskite structure. The concurrent bending of the Mn-O-Mn bond angle inhibits the double-exchange resonance that drives ferromagnetic order and lowers T_C .¹⁰ However, even if the *average* ionic size is kept constant (usually monitored by the so-called tolerance factor), the transition temperature drops as the variance in ionic size increases.³ This suggests that *local* bond-angle bending is more important than the average and that disorder therefore plays a major role. Indeed, there is considerable evidence that metallic and polaronic regions coexist in the vicinity of the phase transition. The phase separation is dynamic, but much slower than is typical for critical fluctuations, as can be seen in noise measurements,^{11,12} muon spin relaxation,¹³ and the presence of strong diffusive peaks in neutron scattering. The case for phase separation, driven by the randomness inherent in the system, has been documented extensively in a recent review by Dagotto *et al.*¹⁴

This paper explores the dramatic changes in thermodynamic behavior that accompany the better known changes in

transport properties upon various substitutions away from $\text{Sr}_{3/8}$. We argue that bond disorder plays a key role and that the problem should be considered in the context of a Griffiths singularity. In his pioneering paper, Griffiths¹⁵ considered a percolationlike problem in which each exchange bond in a system has value J_1 with probability p and $J_2=0$ with probability $1-p$. For all $p < 1$, Griffiths showed that the free energy, and thus the magnetization, is singular at the transition point $T_C(p)$, a consequence of the accumulation of clusters whose local transition temperatures exceed $T_C(p)$. Fisch¹⁶ extended the argument to $0 \leq J_2 < J_1$, demonstrating that the singularities persist. These results suggest, as emphasized by Dotsenko,¹⁷ that the essential contributions of local minima destroy the length-scaling picture of a random-fixed-point universality class. Bray and Moore¹⁸ and Bray¹⁹ extended the argument to any bond distribution that reduces the transition temperature from some “pure” value T_G and proposed a distribution function for eigenvalues of the inverse-susceptibility tensor that captures the singularity proposed by Griffiths. Bray terms the temperature range $T_C(p) \leq T \leq T_G$ the Griffiths phase, where p is now a measure of the bond distribution. The nature of the Griffiths singularity in the limit of small dilution has been treated in some detail in the quantum limit where $T_C(p) \rightarrow 0$ by Castro Neto and co-workers.^{20,21}

In this paper, which builds upon earlier work,²² we demonstrate the progression of the magnetic and thermodynamic properties of doped LaMnO_3 as the transition temperature is lowered from its maximum value. We then turn to an analysis of the low-field behavior of the magnetization based on the inverse-susceptibility eigenvalue distribution proposed by Bray. In Sec. IV, we extend the analysis by introducing a bond distribution that changes with temperature and field as a consequence of the double-exchange mechanism and treat it using a cluster model. Section V concludes the paper with a discussion of the implications of this analysis for disordered double-exchange magnets.

II. MAGNETIC AND THERMODYNAMIC PROPERTIES

Three single-crystal samples were used in this study. Two samples, $\text{La}_{0.7}\text{Sr}_{0.3}\text{MnO}_3$ (LSMO) and $\text{La}_{0.7}\text{Ca}_{0.3}\text{MnO}_3$ (LCMO), were grown by optical floating-zone techniques by Okuda *et al.*²³ A sample of $\text{La}_{0.66}(\text{Pb}, \text{Ca})_{0.34}\text{MnO}_3$ (LPMO) was grown by flux methods as described elsewhere²⁴ and has a transition temperature midway between the extremes represented by the other samples. The LSMO and LCMO samples were cut into rectangular slabs with the long direction along the a directions while the LPMO was used as grown, but had a similar orientation. The magnetization of each crystal was measured in a conventional Quantum Design MPMS system with the field along the longest axis of the sample. The data reported are corrected for demagnetization. Following the magnetic measurements, gold current and voltage pads were sputtered on the sample and leads were attached to the pads with silver paint. One end of the sample was varnished to a copper block while a strain gauge heater was attached to the opposite end. A pair of fine-wire thermocouples were connected to measure the temperature differ-

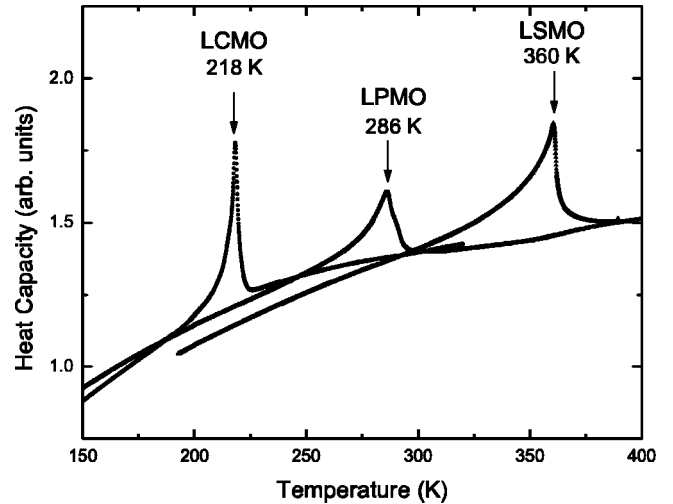


FIG. 1. Heat capacity in zero applied field for the three samples. The $\text{La}_{0.66}(\text{Ca}, \text{Pb})_{0.34}\text{MnO}_3$ sample was damaged upon thinning and shows a reduced heat-capacity peak.

ence between the voltage contacts for thermopower measurements. The resistance and thermopower were measured sequentially at each field-temperature point in a Quantum Design PPMS instrument. Thermopower results have been reported elsewhere.²⁵ Following the transport measurements, the samples were mechanically thinned, removing the gold contact pads, and mounted for ac calorimetry measurements. The small LPMO crystals were damaged in this process and the heat-capacity data in field could not be obtained. Samples were placed in a cryostat in which a magnetic field up to 7 T could be applied. Light from a stabilized quartz lamp was chopped mechanically to provide periodic heat pulses to the sample at the desired frequency. The proper operating point was located at the midpoint of the range where the ensuing temperature oscillations were inversely proportional to the frequency of the heat pulses. A thorough review of the ac method has been prepared by Kraftmakher.²⁶

Figure 1 shows the ac heat capacity vs temperature for the three samples in zero applied field. Although the LPMO sample shows obvious signs of the damage that accompanied thinning, as noted above, the heat capacity exhibits a sharp peak at the temperatures indicated as T_C (heat capacity) in Table I. The heat-capacity curve for LCMO is significantly narrower than for LSMO, a point we address in more detail below. Despite its sharpness, there is no sign of hysteresis in the LCMO data. Similarly, the magnetization curves change significantly as the transition temperature is reduced. As had been reported previously,⁴ the magnetization for LSMO can be collapsed to a single curve using exponents that are simi-

TABLE I. Transition temperatures and critical exponents for samples studied.

	T_C (heat capacity)	T_C (scaling)	β	δ
LCMO	218 K	216.2 K	0.10	16.9
LPMO	286 K	285.1 K	0.24	7.1
LSMO	360 K	359.1 K	0.31	5.1

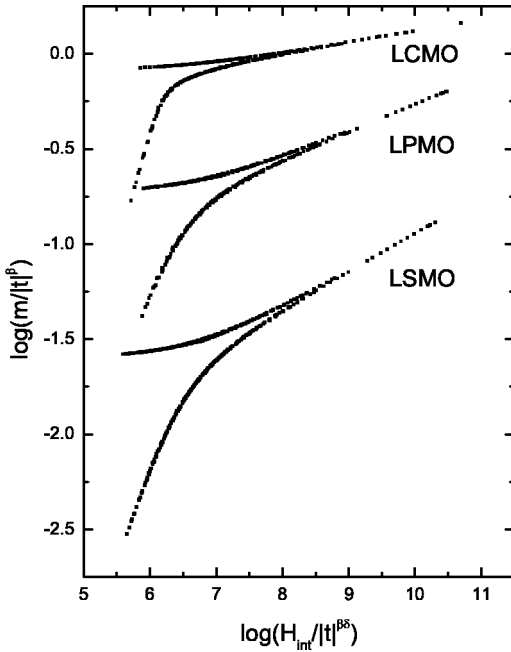


FIG. 2. Scaling curves for the three samples. The exponents β and δ deviate strongly from Heisenberg-like values as T_C is reduced. The temperatures in parentheses indicate the range of data used in the scaling curves.

lar to those expected for a Heisenberg ferromagnet. Our data behave similarly, as can be seen in Fig. 2 with the exponent values given in Table I. Here, $t = (T/T_C - 1)$; the values of T_C , β , and δ are those that best collapse the data above (upper curve) and below (lower curve) T_C . The exponents are somewhat different from those reported by Ghosh *et al.*,⁴ but are not far from the Heisenberg values $\beta = 0.36$ and $\delta = 4.8$. However, as the transition temperature decreases, the data for lower- T_C samples can be collapsed only by using exponents that are far from those for any known universality class.

The effects can be seen more directly by following the magnetization curves along the isotherms corresponding to the peaks in the zero-field heat-capacity curves. The ratio of the measured magnetization at T_C to the low-temperature saturation value is shown in Fig. 3 for all three samples. The solid curves are fits to the usual expression $M(H, T_C) \propto H^{1/\delta}$ along the critical isotherm; the exponents agree with the scaling analysis. Note that the magnetization of LCMO rises to 60% of saturation in low fields, yet shows no signs of hysteresis or remanence. It is tempting to attribute this behavior to a first-order transition, but we discuss it in the next section in terms of a Griffiths singularity.

While the LSMO data seem quite close to Heisenberg behavior, the low-field susceptibility of that sample, as well as that of the others, is anomalous. Figure 4 shows the inverse susceptibility of the three samples, normalized by the low-temperature saturation magnetization $M(0)$ and plotted versus reduced temperature T/T_C . If these data followed a Curie-Weiss law, they would lie on a straight line given by

$$HM(0)/M(T) = \frac{3k_B T_C}{g\mu_B(S+1)} \left(\frac{T}{T_C} - 1 \right). \quad (1)$$

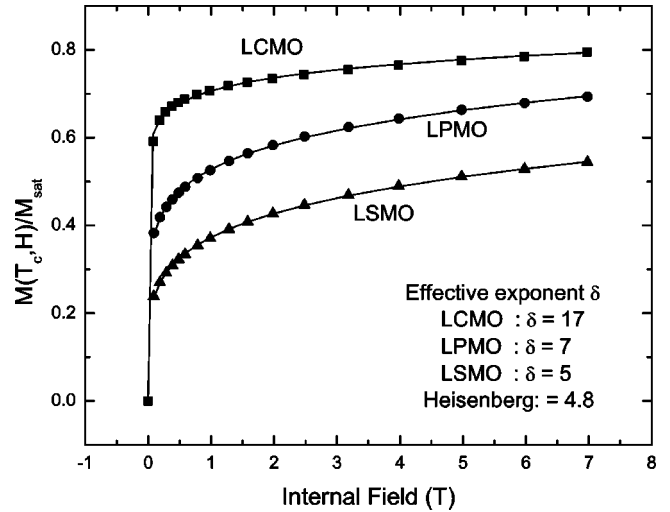


FIG. 3. Magnetization vs internal field along the critical isotherm. The exponent δ increases strongly as the transition temperature decreases.

The dashed line is the slope expected for $T_C = 360$ K and $S = 1.85$, namely, the values for LSMO. The actual slope of the LSMO data corresponds to a spin $S \approx 3.5$ while that for LCMO requires $S \approx 6$. These results indicate the persistence of spin clusters to temperatures significantly above the Curie temperature, even in nominally Heisenberg-like LSMO. Even more dramatic is the sharp downturn or knee in the LCMO inverse-susceptibility data and, to a lesser but still noticeable extent, in those for LPMO. This downturn, reported by De Teresa *et al.*,²⁷ moves to higher temperatures with increasing field. The scaling analysis shown in Fig. 2 includes data only for $T/T_C \leq 1.06$, that is, at temperatures below the downturn. We defer discussion of the other lines in Fig. 4 to the next section.

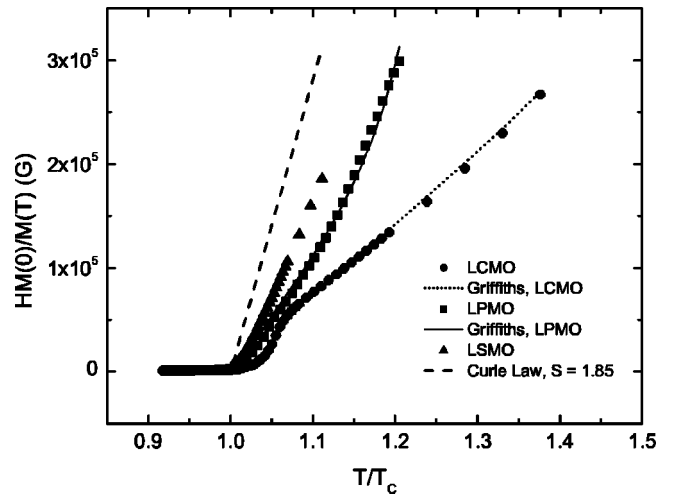


FIG. 4. Inverse susceptibility multiplied by the saturation magnetization. The dashed curve is the Curie-Weiss susceptibility expected for $S = 1.85$ and the critical temperature of the LSMO sample. The effective slope for LSMO corresponds to $S \approx 3.5$, increasing to $S \approx 6$ for LCMO. The curves through the data points are for the Griffiths model, as described in the text.

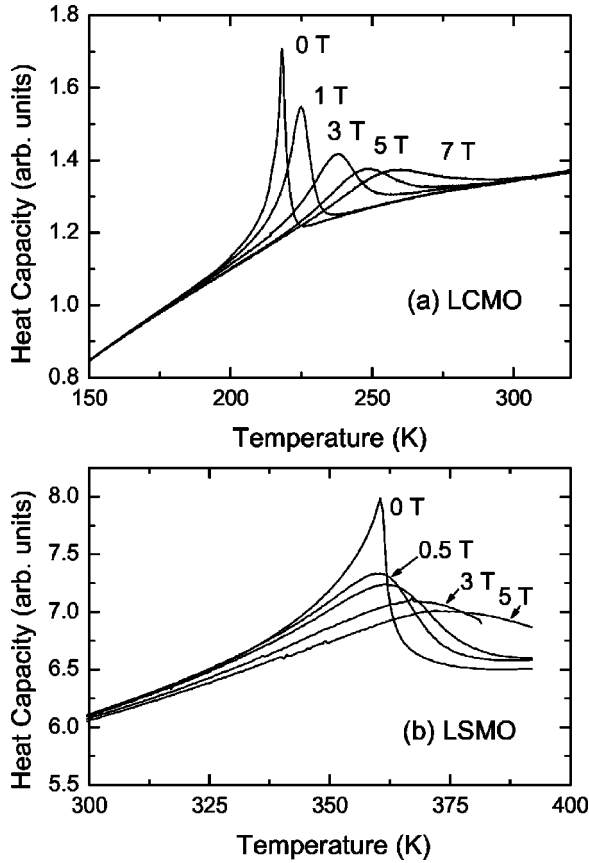


FIG. 5. Field dependence of the heat capacity of (a) LCMO and (b) LSMO at the listed fields. The curve for $B=1$ T is not labeled in (b). Note the qualitatively different behavior of the two samples.

The anomalies in the magnetization are, of course, mirrored in the field dependence of the heat capacity. Figure 5(a) shows the data for LCMO and Fig. 5(b), for LSMO at a succession of applied fields. The LCMO data shift to higher temperature while remaining relatively narrow, while the LSMO data, like those of most ferromagnets, broaden with little shift in peak position. The heat-capacity data, like the magnetization, should collapse to a universal curve when scaled with a power of the magnetic field and plotted versus scaled temperature according to

$$[C(H,T) - C(0,T)]H^{\alpha/\beta\delta} = f\left(\frac{t}{H^{1/\beta\delta}}\right). \quad (2)$$

As we reported earlier,²⁸ neither the exponents that provide a scaling collapse of the magnetization data, nor any other set that we can identify, are able to satisfy the scaling conditions for LCMO. This is shown in Fig. 6(a). However, the LSMO data, Fig. 6(b), do fall on a single scaling curve using the values of β and δ from the magnetization scaling, and $\alpha = -0.1$; the last differs somewhat from a value consistent with β and δ . As the susceptibility data of Fig. 4 demonstrate, even LSMO does not exhibit single-spin behavior, so we must take the critical exponents to represent only effective values.

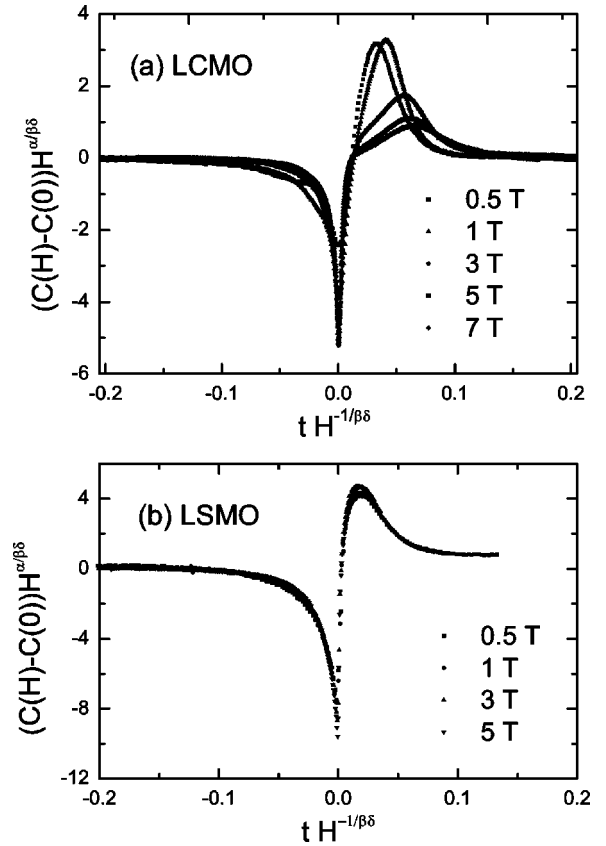


FIG. 6. The deviation of the heat capacity in magnetic field from its zero-field value, scaled by field and plotted versus scaled reduced temperature. No set of exponents can be found to collapse the LCMO data in (a) to a single curve. By contrast, the same values of β and δ used in Fig. 3, along with $\alpha = -0.1$, serve to collapse the LSMO data in (b).

III. GRIFFITHS-PHASE ANALYSIS: SUSCEPTIBILITY

In his pioneering 1969 paper, Griffiths¹⁵ demonstrated that the magnetization of a randomly diluted ferromagnet above its percolation point is a nonanalytic function of the field at all temperatures below the pure-system Curie temperature. The argument was extended to alloys, i.e., for $0 \leq J_2 < J_1$, by Fisch¹⁶ and to any positive-definite (bounded) distribution of exchange interactions by Bray and Moore.¹⁸ In the latter paper, the authors focused on the distribution $\rho(\lambda)$ of the eigenvalues λ of the inverse-susceptibility matrix. Above the critical temperature T_C but below the highest achievable critical temperature T_G , all states with small values of λ are localized; there are local regions of large susceptibility, but no long-range order. Just at T_C , an extended state of infinite susceptibility ($\lambda=0$) appears, signaling the sudden onset of long-range order. Subsequently, Bray¹⁹ suggested an explicit form for this distribution,

$$\rho(\lambda) \propto \lambda^{-x} \exp[-A(T)/\lambda]. \quad (3)$$

The power-law prefactor was not specified in that paper, but Bray and Huifang²⁹ later considered a soluble model of the diluted Ising ferromagnet and verified Eq. (3) with $x=1/2$. The amplitude A was argued to diverge as $(1-T/T_G)^{-2\beta}$ at

TABLE II. Parameters used in Griffiths susceptibility calculation.

	a (K)	x	T_C (K)	T_G (K)
LCMO	5.0	0.53	224.8	376
LPMO	4.15	0.61	293.5	365

the pure, or Griffiths, temperature T_G and to vanish as $(T/T_C - 1)^{2(1-\beta)}$ at the actual Curie point. The exponent β is the usual exponent for the system at its pure transition. This distribution peaks at $\lambda = A/x$ and vanishes at $\lambda = 0$ for all temperatures above T_C . There is, therefore, a pileup of small eigenvalues—large susceptibilities—as the Curie temperature is approached. Just at T_C the distribution collapses into $\lambda = 0$ causing the magnetization to jump to a large value in applied field—the hallmark of the Griffiths singularity.

We assert here that the transition temperatures evidenced in the sequence LSMO, LPMO, and LCMO are a consequence of increased randomness due to the increased local bond bending in the vicinity of successively smaller dopant atoms. If so, then each sample is farther below the Griffiths temperature of an optimal system and will consequently exhibit a broader temperature range over which $A(T)$ varies between its zero at T_C and its divergence at T_G . We calculate the average susceptibility from Eq. (3) according to

$$\bar{\chi} = C \frac{\int_0^T \lambda^{-1} \rho(\lambda) d\lambda}{\int_0^T \rho(\lambda) d\lambda}, \quad (4)$$

where $C = ng^2 \mu_B^2 S(S+1)/3k_B$ is the Curie constant and the upper limit of the integral recognizes that the smallest susceptibility at any temperature is C/T for spin S . The exponential amplitude is taken to be

$$A(T) = a \frac{(T/T_C - 1)^{2(1-\beta)}}{(1 - T/T_G)^{2\beta}}, \quad (5)$$

with $\beta = 0.38$ and a, T_C, T_G , and x varied to fit the susceptibility data. The downturn in the inverse-susceptibility curves sets the value of T_C while the upward curvature is controlled by T_G . There is considerable covariance of the amplitude a and prefactor exponent x , so the values are subject to some uncertainty. We use the effective spin $S = 1.85$ appropriate for 70% $S = 2$ and 30% $S = 1.5$. Because the downturn (if there is one) for LSMO is not discernible, we cannot get an unambiguous fit for those data. However, the solid curve for LPMO and dotted curve for LCMO in Fig. 4 are reliable, with the parameter values given in Table II.

Of considerable interest is the fact that the Griffiths temperatures that emerge from the fits are comparable and only slightly above the observed T_C for LSMO. This indicates that LSMO lies very close to the optimal critical temperature and explains why it can be treated in the context of an ordinary Heisenberg ferromagnet, albeit with slightly modified critical exponents.

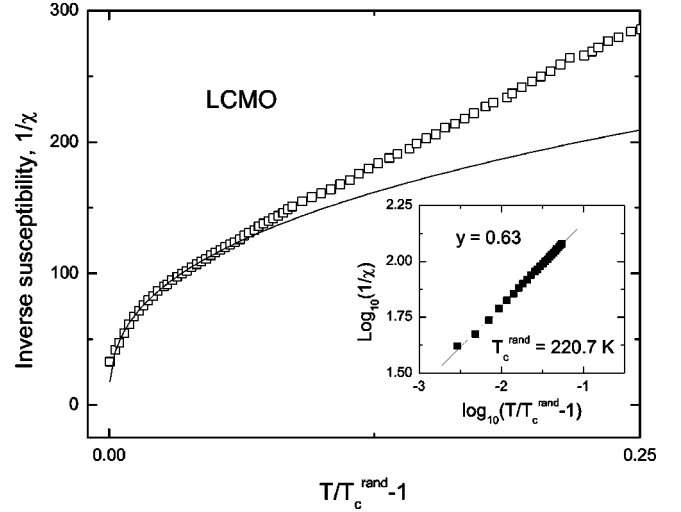


FIG. 7. Inverse susceptibility of LCMO at 500 Oe as a function of T/T_c . The solid curve in the main figure and the logarithmic plot in the inset is a fit of the data to a power law with the result that $y = 0.63$.

Note that the critical temperature obtained from the Griffiths fit is somewhat higher than that obtained from scaling or the heat capacity. This may reflect the suggestion made by Griffiths in his original paper that the susceptibility would tend to diverge in advance of the onset of long-range order. To examine this, we focus on the downturn in the inverse susceptibility for LCMO. In recent work on f -electron compounds in which disorder has driven T_C to 0 K, Castro Neto *et al.*²⁰ have argued that the susceptibility diverges as T^{y-1} where $y \leq 1$ is related to the tunneling barrier for a cluster of N aligned spins. In general, the relaxation rate of Griffiths clusters is also expected to be proportional to its inverse susceptibility,¹⁹ so similar arguments might hold here, i.e., $\chi^{-1} \propto (T/T_C - 1)^{1-y}$. In Fig. 7 we plot the low-field susceptibility of the LCMO crystal as a function of T/T_C , with $T_C = 220.7$ K obtained by fitting the data to a power law. The random critical temperature is much closer to that indicated by the heat-capacity peak, and is a more reliable measure of the tendency of the inverse susceptibility to vanish with an exponent $y = 0.63$, that is, to approach T_C with infinite slope. Though closer to the heat-capacity peak (218.2 K at this field) it appears to be somewhat above the temperature at which long-range order is established, as suggested by Griffiths.

IV. GRIFFITHS-PHASE ANALYSIS: HEAT CAPACITY

In the classic Griffiths-phase model, exchange interactions are distributed randomly, but once distributed, are fixed. This is not the case for a double-exchange system in which the effective coupling between two Mn ions depends on the alignment of their respective core spins or, equivalently, the rate at which the outer e_g electron hops between the two ions. As a consequence, as spins order locally, the spin clusters are also more metallic, and the combined effect is to reinforce and stabilize the formation of large Griffiths clusters. In the presence of an applied magnetic field, these

metallic, spin-aligned clusters form at higher temperatures, strongly affecting the thermodynamics of the transition and, of course, giving rise to the CMR effect itself.

The heat capacity associated with the Griffiths singularity was studied for the random spherical model by Rauh,³⁰ who found a jump singularity at T_C . We take a different approach here, using the Oguchi model³¹ to calculate the magnetization and the associated short-range order parameter. In this approach, the interaction energy of a pair is calculated exactly using the double-exchange energy

$$E_{de}(S_i) = -xt \frac{S_i + 1/2}{2S + 1} - \overline{E_{de}(S_i)}, \quad (6)$$

where the bar denotes an average over all possible values of the total spin $1/2 \leq S_i \leq 7/2$ of the two $S = 3/2$ cores and the shared e_g electron of the pair. The pair interacts with its $z - 1$ neighbors through an effective magnetic field

$$H_{eff}(H, T) = H + 2(z - 1)S\{c(H, T)J_{met} + [1 - c(H, T)]J_{ins}\}m(H, T). \quad (7)$$

Here, $m(H, T)$ is the reduced magnetization to be calculated, J_{met} is the exchange interaction in metallic regions that have a concentration $c(H, T)$, and J_{ins} is the exchange energy in nonmetallic (but still conductive) regions. The insulating exchange energy can be extracted directly from the inverse susceptibility by extrapolating the linear region of Fig. 4 to obtain the Curie temperature $\Theta = 202$ K, from which mean-field theory gives $J_{ins} = 0.85$ meV. We obtain J_{met} from the spin-wave dispersion of manganites which is $D \approx 160$ meV \AA^2 independent of concentration. The effective Heisenberg exchange interaction giving this spin-wave stiffness is $J_{met} = D/2S_{eff}a^2 = 1.56$ meV; here $S_{eff} = 1.85$ is the average spin per manganese atom. The hopping energy giving the same spin-wave spectrum is $t = D(2S + 1)/xa^2 = 140$ meV.³² Alternatively, we can use the critical temperature from Monte Carlo simulations $k_B T_C \approx 0.14t$,³³ obtaining $t = 134$ meV.

The most important input into the model is the relative concentration of metallic bonds. We obtain this empirically from the resistivity data as outlined in Fig. 8. The zero-field data at low temperature are fit to the power law

$$\rho_{lt} = \rho_0 + a_2 T^2 + a_5 T^5, \quad (8)$$

and the high-temperature data to an adiabatic small-polaron contribution,

$$\rho_{ht} = bT \exp(E_p/T), \quad (9)$$

as done previously.³⁴ Here, however, the metallic fraction is obtained by solving the generalized effective-medium (GEM) expression³⁵ using the experimental resistivity ρ_{exp} and the extrapolated high- and low-temperature fits. The GEM analysis differs from that used in Ref. 22, guaranteeing that percolation occurs at a critical concentration c_c that we set to the 3D value for spherical inclusions, namely, $c_c \approx 1/6$. The equation to be solved for $c(H, T)$ is

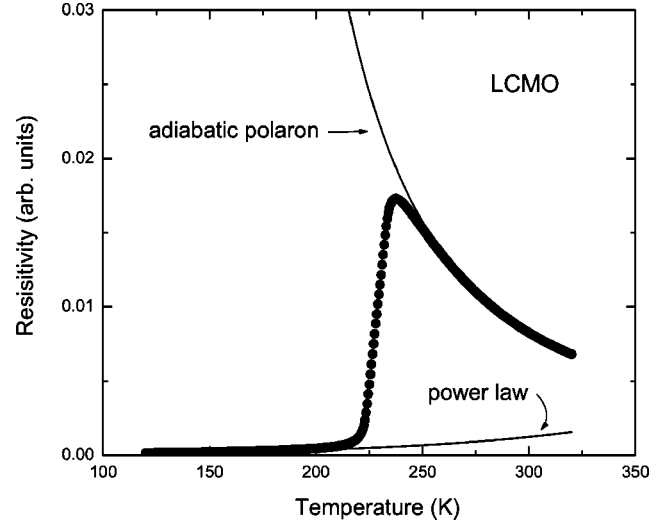


FIG. 8. Resistivity of the LCMO sample in a field of 1 T. Superposed are the fits to the zero-field data at low temperatures to a power law and at high temperatures, to an adiabatic small-polaron model.

$$c(H, T) \frac{\rho_{exp}^{1/t} - \rho_{lt}^{1/t}}{\rho_{exp}^{1/t} + A\rho_{lt}^{1/t}} + [1 - c(H, T)] \frac{\rho_{exp}^{1/t} - \rho_{ht}^{1/t}}{\rho_{exp}^{1/t} + A\rho_{ht}^{1/t}} = 0, \quad (10)$$

where $A = (1 - c_c)/c_c$ and the percolation exponent is set to $t = 2$. Several resistivity curves and the resulting concentrations are shown in Fig. 9.

We proceed by calculating the magnetization self-consistently in the context of the Oguchi model, that is, we solve

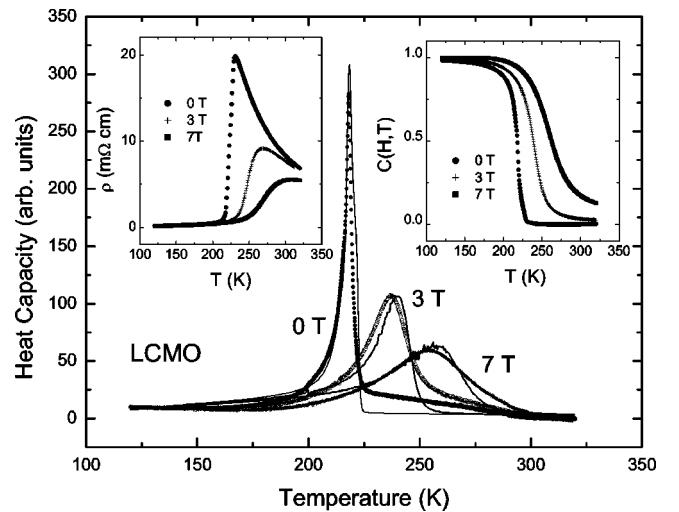


FIG. 9. Heat-capacity curves calculated from the Oguchi model at several fields. The metallic concentrations extracted from the resistivity curves (left inset), using the GEM analysis, are shown in the right inset. The only other input is the overall amplitude of the zero-field curve. The calculated curves differ from those presented in Ref. 22.

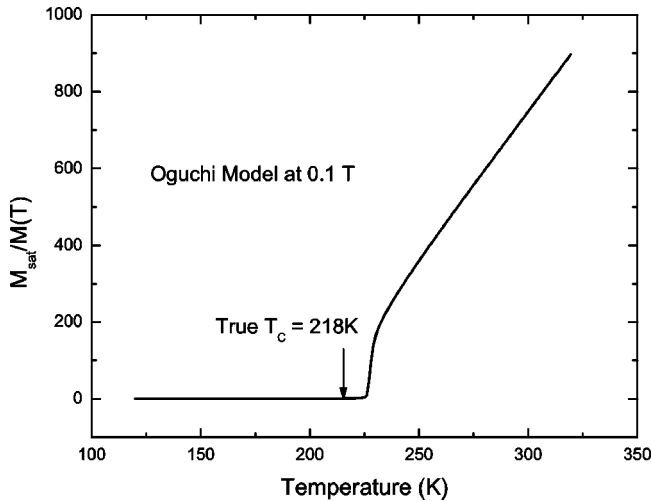


FIG. 10. Inverse susceptibility at low field calculated using the Oguchi model. The sharp downturn at a temperature above the peak in the heat-capacity peak mirrors the behavior of the experimental data.

$m(H, T)$

$$= \frac{1}{Z} \sum_{S_i=1/2}^{7/2} \sum_{p=S_i} p \exp \left[\frac{-E_{de}(S_i) + pg \mu_B H_{eff}(H, T)}{k_B T} \right], \quad (11)$$

where Z is the partition function (same sum without the factor p). Once $m(H, T)$ is known, we compute the energy density by averaging $E_{de}(S_i)$ at each field/temperature point using the Boltzmann factors that have been calculated self-consistently, and differentiate numerically to obtain the heat capacity. The amplitude is chosen to fit the zero-field data and kept constant for other fields. The results, shown in Fig. 9, provide a better representation of the metallic fraction than the simple percolation approach used in Ref. 22. The width, amplitude, and shift in temperature of curves at successive fields agree extremely well with the data. In each case, the experimental peaks are broader on the high-temperature side of the curve, indicating that the Oguchi calculation underestimates the persistence of short-range order at higher temperatures. Nonetheless, the curves show quite clearly that the metallic concentrations extracted from the GEM analysis are able to predict the unusual critical behavior of LCMO.

The final question in this analysis is whether the Oguchi model described here actually reproduces Griffiths-like behavior at low fields. The magnetization has been calculated at the same fields as the data in Fig. 4, using the zero-field value $c(0, T)$ extracted from the resistivity. The result is shown in Fig. 10. Note that the downturn in advance of the heat-capacity peak is similar to the experimental data. The Oguchi approach does not capture the presence of large spin clusters and therefore does not produce upward curvature in the inverse susceptibility.

V. CONCLUSION

The nature of the ferromagnetic-paramagnetic transition in these materials has been the subject of considerable dis-

ussion for decades. Most recently, Kim *et al.*³⁶ argued for a tricritical point just above $x=0.33$ in $\text{La}_{1-x}\text{Ca}_x\text{MnO}_3$. They do not identify the two phase lines that should emanate from the tricritical point. Further, examination of their $x=0.33$ data shows that the susceptibility at 290 K corresponds to a spin $S=3.5$, rather than the $S \leq 2$ expected. Consequently, even 30 K above the transition there is evidence for clustering, a signature of the Griffiths behavior we propose here. Apart from the critical behavior, various explanations for the CMR phenomenon draw upon elements of the Griffiths-phase approach—mixed phases and phase separation, percolation, and slow dynamics—but have not connected them to produce a coherent picture. In particular, the dramatic changes in behavior that accompany subtle changes in the size and concentration of dopant atoms have not been adequately treated. We have attempted here to demonstrate that the intrinsic randomness introduced by substituting ions that differ in size (and of course valence) from the usual A-site atom drive the system from its optimal doping and ionic size at $\text{Sr}_{3/8}$ to the strong CMR regime as Sr is changed to Pb and finally Ca. Remarkably, the transition to the magnetic phase remains second orderlike, by which we mean that the properties are fully reversible and, with the exception of the heat capacity, can be treated by the usual ferromagnetic scaling equations, albeit with nonuniversal (even bizarre) values for the critical exponents.

Outside the “critical” regime, there is ample evidence in our data, and in a wealth of further data in the literature, to demonstrate coexistence of more or less metallic and more or less insulating regions over a wide temperature range both above and below the Curie temperature. We have shown that the clusters evolve as the temperature is reduced toward T_C in a manner consistent with the theoretical ideas of Bray and Moore¹⁸ and Bray.¹⁹ In essence, the transition is not primarily a question of connectedness and the evolution of a tenuous infinite cluster, but rather more a homogeneous nucleation problem in which the most-probable cluster size grows as the temperature is reduced until the numerous large clusters become effectively space filling, providing an abrupt onset of nearly complete long-range order.

The situation in the manganites differs significantly from a straightforward ideal Griffiths phase precisely because Griffiths clusters that form are more metallic and therefore have stronger ferromagnetic double-exchange energies than the surrounding matrix. The CMR effect thus reinforces cluster formation: local spin ordering increases the mobility of electrons, which then increases local exchange interactions via double exchange, which in turn feeds back to lock in local spin ordering. We have attempted to deal with this effect phenomenologically by determining the fraction of metallic, high-susceptibility clusters from the field- and temperature-dependent resistivity using a generalized effective-medium approach. Knowing that fraction, we compute an effective magnetic field acting on each pair of double-exchange-coupled spins and from that, determine the magnetization and energy density. We demonstrate that this approach accurately tracks the height and temperature of the peak in the heat capacity and, to a significant extent, its width. We regard the unusual behavior of the heat capacity in

magnetic field, along with the strongly non-Curie-Weiss behavior of the susceptibility to be hallmarks of the CMR effect, as important in understanding it as the more dramatic changes in transport properties.

Our analysis of the CMR transition in terms of Griffiths-phase ideas provides an understanding of the evolution of behavior from LSMO, whose Curie point is near the Griffiths temperature, to LCMO, which exhibits Griffiths-phase and magnetotransport signatures. However, the interplay of local order and enhanced double exchange requires empirical input and remains, therefore, unsatisfactory. We still need to understand the mechanism by which Griffiths clusters order in a polaronic, double-exchange magnet, and how that pro-

cess assists in stabilizing large clusters. It is our hope that this paper has helped to delineate the problems that remain.

ACKNOWLEDGMENTS

This material is based upon work supported by the U.S. Department of Energy, Division of Materials Sciences under Award No. DEFG02-91ER45439, through the Frederick Seitz Materials Research Laboratory at the University of Illinois at Urbana-Champaign. We are especially grateful for the crystals provided by T. Okuda, Y. Tomioka, and A. Asamitsu in the group of Professor Y. Tokura. We have also benefited from discussions with Marcelo Jaime, Yuli Lyanda-Geller, and Paul Goldbart.

*Electronic address: salamon@uiuc.edu

†Electronic address: schun@sejong.ac.kr

¹M.B. Salamon and M. Jaime, *Rev. Mod. Phys.* **73**, 583 (2001).

²H. Hwang, S.-W. Cheong, P. Radaelli, M. Marezio, and B. Batlogg, *Phys. Rev. Lett.* **75**, 914 (1995).

³L. Rodriguez-Martinez and J. Attfield, *Phys. Rev. B* **54**, R15 622 (1996).

⁴K. Ghosh, C. Lobb, R. Greene, S. Karabashev, D. Shulyatev, A. Arsenov, and Y. Mukovskii, *Phys. Rev. Lett.* **81**, 4740 (1998).

⁵C. Zener, *Phys. Rev.* **2**, 403 (1951).

⁶A. Urushibara, Y. Moritomo, T. Arima, A. Asamitsu, G. Kido, and Y. Tokura, *Phys. Rev. B* **51**, 14 103 (1995).

⁷A. Millis, P. Littlewood, and B.I. Shraiman, *Phys. Rev. Lett.* **74**, 5144 (1995).

⁸A.J. Millis, R. Mueller, and B.I. Shraiman, *Phys. Rev. B* **54**, 5405 (1996).

⁹M. Jaime, M.B. Salamon, M. Rubinstein, R.E. Trece, J. Horwitz, and D.B. Chrisey, *Phys. Rev. B* **54**, 11 914 (1996).

¹⁰J.L. Garcia-Munoz, J. Fontcuberta, M. Saaaidi, and X. Obradors, *J. Phys.: Condens. Matter* **8**, L787 (1996).

¹¹V. Podzorov, M. Uehara, M.E. Gershenson, T.Y. Koo, and S.-W. Cheong, *Phys. Rev. B* **61**, 3784 (2000).

¹²R. Merithew, M. Weissman, F. Hess, P. Spradling, E. Nowak, J. O'Donnell, J. Eckstein, Y. Tokura, and Y. Tomioka, *Phys. Rev. Lett.* **84**, 3442 (2000).

¹³R. Heffner, J. Sonier, D. MacLaughlin, G. Nieuwenhuys, G. Ehlers, F. Mezei, S. Cheong, J. Gardner, and H. Roder, *Phys. Rev. Lett.* **85**, 3285 (2000).

¹⁴E. Dagotto, T. Hotta, and A. Moreo, *Phys. Rep.* **344**, 1 (2001).

¹⁵R.B. Griffiths, *Phys. Rev. Lett.* **23**, 17 (1969).

¹⁶R. Fisch, *Phys. Rev. B* **24**, 5410 (1981).

¹⁷V.S. Dotsenko, *J. Phys. A* **32**, 2949 (1999).

¹⁸A.J. Bray and M.A. Moore, *J. Phys. C* **15**, L765 (1982).

¹⁹A.J. Bray, *Phys. Rev. Lett.* **59**, 586 (1987).

²⁰A.H. Castro Neto, G. Castilla, and B.A. Jones, *Phys. Rev. Lett.* **81**, 3531 (1998).

²¹A.H.C. Neto and B.A. Jones, *Phys. Rev. B* **62**, 14 975 (2000).

²²M.B. Salamon, P. Lin, and S.H. Chun, *Phys. Rev. Lett.* **88**, 197203 (2002).

²³T. Okuda, Y. Tomioka, A. Asamitsu, and Y. Tokura, *Phys. Rev. B* **61**, 8009 (2000).

²⁴M. Jaime, P. Lin, M.B. Salamon, and P.D. Han, *Phys. Rev. B* **58**, R5901 (1998).

²⁵P. C.-Y. Lin, Ph.D. thesis, University of Illinois, 2001.

²⁶Y. Kraftmakher, *Phys. Rep.* **356**, 1 (2002).

²⁷J.M. De Teresa, M.R. Ibarra, P.A. Algarabel, C. Ritter, C. Marquina, J. Blasco, J. Garcia, A. del Moral, and Z. Arnold, *Nature (London)* **386**, 256 (1997).

²⁸P. Lin, S.H. Chun, M.B. Salamon, Y. Tomioka, and Y. Tokura, *J. Appl. Phys.* **87**, 5825 (2000).

²⁹A.J. Bray and D. Huifang, *Phys. Rev. B* **40**, 6980 (1989).

³⁰A. Rauh, *Phys. Rev. B* **14**, 1997 (1976).

³¹J. S. Smart, *Effective Field Theories of Magnetism* (Saunders, Philadelphia, 1966).

³²N. Ohata, *J. Phys. Soc. Jpn.* **34**, 343 (1973).

³³M.J. Calderon and L. Brey, *Phys. Rev. B* **58**, 3286 (1998).

³⁴M. Jaime, P. Lin, S.H. Chun, M.B. Salamon, P. Dorsey, and M. Rubinstein, *Phys. Rev. B* **60**, 1028 (1999).

³⁵G. Hurvits, R. Rosenbaum, and D.S. McLachlan, *J. Appl. Phys.* **73**, 7441 (1993).

³⁶D. Kim, B. Revaz, B.L. Zink, F. Hellman, J.J. Rhyne, and J.F. Mitchell, *Phys. Rev. Lett.* **89**, 227202 (2002).